N O T I C E

THIS DOCUMENT HAS BEEN REPRODUCED FROM
MICROFICHE. ALTHOUGH IT IS RECOGNIZED THAT
CERTAIN PORTIONS ARE ILLEGIBLE, IT IS BEING RELEASED
IN THE INTEREST OF MAKING AVAILABLE AS MUCH
INFORMATION AS POSSIBLE

RESULTS AND INTREPRETATION OF MEASUREMENTS OF THE LIGHT FLUX IN THE NEAR-SURFACE LAYER OF THE VENUSIAN ATMOSPHERE

Yu. M. Golovin, B. Ye. Moshkin and A.P.E. Ekonomov

Introduction

Unitypical photometers were mounted on the descent vehicles of the automatic interplanetary Venera-9 and Venera-10 stations; these measure the light flux coming from the entire upper hemisphere, from the zenith and from below at an angle $\xi = 23°$ to the nadir in five spectral ranges; in this way, each instrument has 15 independent measurement channels. The average spectral characteristics $S_{ij}(\lambda)$ and the beam patterns $F_{ij}(\theta)$ are shown in Figures 1 and 2. On these drawings, and in the entire work, the first index i is defined as the type of beam pattern and the second, j--is the spectral range; each measurement channel has symbols: i, j, where $i = 1, \ldots 3$; $j = 1, \ldots 5$. Preliminary measurement results were published in references [1, 2] after which the authors conducted full processing of the measurement results obtained.

In this work that part which applies to the near-surface layer of the atmosphere is presented, that is, the field where measurements make it possible to determine the photometric conditions on the surface and certain properties of the surface itself.

RESULTS AND INTERPRETATION OF MEASUREMENTS
OF THE LIGHT FLUX IN THE NEAR-SURFACE LAYER
OF THE VENUSIAN ATMOSPHERE

Yu. M. Golovin, B.Ye. Moshkin, A. P. E. Ekonomov

1. Intensity of radiation incoming to the surface.

The intensity of radiation $J(\lambda,\theta)$ equals the energy of the light flux normally incident per unit of area at an angle θ to the nadir at a single solid angle and in a single interval of wave length $(\lambda,\lambda+d\lambda)$. Close to the surface of the planet, the intensity of radiation does not depend on the azimuth.

The photometers measure intensity of radiation W_{ij}, averaged according to the i-beam pattern and the j spectral characteristic:

$$W_{ij} = \frac{\int_0^\infty S_{ij}(\lambda)\,d\lambda \int_0^{2\pi} d\varphi \int_{-1}^1 J(\lambda,\eta,\varphi) F_{ij}(\eta,\varphi)\,d\eta}{\int_0^\infty S_{ij}(\lambda)\,d\lambda \cdot \int_0^{2\pi} d\varphi \int_{-1}^1 F_{ij}(\eta,\varphi)\,d\eta},\qquad (1)$$

where $\eta=\cos\theta$. The intensity of infinite radiation $0<\eta<1$ we designate by $J\downarrow(\lambda,\eta)$, and the intensity of ascending radiation -- $1<\eta<0$, by $J\uparrow(\lambda,\eta)$. With a large optical thickness of the atmosphere, with conservative scattering and a small albedo of the ground, angular distribution of radiation incident on the surface hardly depends on λ and the function $J\downarrow(\lambda,\eta)$ can be presented in the form

$$J\downarrow(\lambda,\eta) = J\downarrow(\lambda)\, u\downarrow(\eta)\,. \qquad (2)$$

---

*Numbers in the margin indicate pagination in the foreign text.

The function U↓(η), according to {3,4}, equals

$$U_o{\downarrow}(\eta) = \frac{1}{2}(1+A) + \frac{3}{4}(1-A)\eta,$$ (3)

where A -- is the albedo of the ground equal, as we will see later on, to 0.1±0.05.

The ratio of intensities averaged according to the beam pattern of $F_{1j}(\eta)$ and $F_{2j}(\eta)$ (see figure 2), is calculated according to the formula

$$\frac{W_{1j}}{W_{2j}} = \frac{\int_o^1 F_{1j}(\eta)\, U{\downarrow}(\eta)\, d\eta}{\int_o^1 F_{2j}(\eta)\, U{\downarrow}(\eta)\, d\eta} \times \frac{\int_o^1 F_{2j}(\eta)\, d\eta}{\int_o^1 F_{1j}(\eta)\, d\eta},$$ (4)

where U↓(η) is defined by expression (3), as equal to 0.85. The value of this ratio averaged for the entire spectral range of both instruments ($\overline{W_{1j}/W_{2j}}$) equals 0.80±0.05. The coincidence of both values within the limits of measurement error supports the possibility of selecting function U↓(η) in the form (3).

For calculation of J↓(λ) five values of averaged intensities $\overline{W}_j$ are used equal to

$$\overline{W}_j = 0.5\left(W_{1j}(0) + (\overline{W_{1j}/W_{2j}}) \cdot W_{2j}(0)\right),$$ (5)

where $W_{1j}(0)$ and $W_{2j}(0)$ are readings of channels 1j and 2j at the moment of landing. When constructing the function J↓(λ) it is assumed that its graph must pass through point $(\overline{W}_j, \overline{\lambda}_j)$, where $\overline{\lambda}_j$ -- is the effective value of the wavelength, and which fulfills the condition of an insignificant amount of discrepency:

2

$$\left| \frac{\int_0^{\infty} \mathcal{J}\nu(\lambda)\, S_j(\lambda)\, d\lambda}{\int_0^{\infty} S_j(\lambda)\, d\lambda} - \overline{W_j} \right| \approx 0. \tag{6}$$

The values $\overline{\lambda}_j$ are found by a method of sequential approximations and as the first approximation the first standardized moments of spectral characteristics are taken ($\overline{\lambda}_j = \dfrac{\int \lambda S_j(\lambda) d\lambda}{\int S_j(\lambda) d\lambda}$, and the succeeding are calculated according to the formula

$$\mathcal{J}\nu^{(k-1)}\left(\overline{\lambda}_j^{(k)}\right) = \frac{\int_0^{\infty} \mathcal{J}\nu^{(k-1)}(\lambda) S_j(\lambda)\, d\lambda}{\int_0^{\infty} S_j(\lambda)\, d\lambda}. \tag{7}$$

to fulfillment of condition (6) within the limits of measurement error. The results obtained are shown in figure 3.

Irradiance of the surface P and intensity of illumination E are /6 calculated according to the formulas

$$P = \pi \int_{0.5}^{1} \mathcal{J}\nu(\lambda)\, d\lambda, \tag{8}$$

$$E = 681\pi \int_{0.4}^{0.7} \mathcal{V}(\lambda) \cdot \mathcal{J}\nu(\lambda)\, d\lambda, \tag{9}$$

where $v(\lambda)$ -- is the spectral sensitivity of the mean eye, and amounts to:

Venera - 9, $P = 83$ W/m^2 $E = 10,500$ lux

Venera - 10, $P = 61$ W/m^2 $E = 6900$ lux.

One should note that the spectral composition of the light flux incident on the surface corresponds to an orange color.

2. Coefficient of Scattering of the Atmosphere and Evaluation of the Surface Relief.

3

The relationships of measured intensities W_{1j} to altitude over the surface are the initial material for determining the coefficient of scattering of the atmosphere close to the surface. The measured values W_{1j} and W_{3j} are presented in figures 4-7. The time to the moment of landing and the altitude over the surface in a uniform atmosphere are applied on the axis of the abscissa in all the drawings. The clearly expressed periodic components on the curves W_{3j} (Venera-9, figure 5) are explained by rotation of the descent vehicle with a period of about 30 s around its axis of symmetry with the condition that if the surface is horizontal then the axis of rotation of the vehicle is not vertical or the axis of rotation of the vehicle is vertical, but the surface has a certain slope.

Naturally there are possible and intermediate variations; however, the absence of direct data on orientation of the vehicle does not make it possible to make an unambiguous selection of the descent model.

An equation for intensity of the ascending light flux in the direction $\arccos \eta$ has the form

$$J\!\uparrow(\tau, \eta, \lambda) = \int_0^\tau B(\tau', \eta, \lambda)\, e^{-\frac{(\tau-\tau')}{|\eta|}} |\eta|^{-1} d\tau' + R(\lambda)\, e^{-\frac{\tau}{|\eta|}}, \qquad (10)$$

where
$$B(\tau', \eta, \lambda) = \frac{\omega}{4\pi} \int_0^{2\pi} d\varphi \int_{-1}^{1} J(\tau', \eta', \lambda)\, x(\gamma)\, d\eta'$$

(11)

-- is the function of sources, τ-- is optical thickness calculated from the surface vertically, $R(\lambda)$ is brightness of the surface, ω-- is the albedo of a single scattering, $x(\gamma)$ -- is the indicatrix of

4

scattering, and then it was assumed that

$$x(\gamma) = \frac{3}{4}(1 + \cos^2\gamma),\tag{12}$$

α-- is the angle between the incident and scattered beam

$$\cos\gamma = \eta \eta' + \sqrt{(1-\eta^2)[1-(\eta')^2]}\,\cos\varphi,\tag{13}$$

where ϕ-- is the azimuthal angle.

The functions $J(\tau',\eta'\lambda)$ in formula (11) can be presented as the total of descending and ascending light flux:

$$J(\tau',\eta',\lambda) = J\!\downarrow(\tau',\lambda)\cdot U\!\downarrow(\eta') + J\!\uparrow(\tau',\lambda)\cdot U\!\uparrow(\eta'),\tag{14}$$

where $U\!\downarrow(\eta')$ is defined by formula (3) and $U\!\uparrow(\eta')$ can be presented in the form

$$U\!\uparrow(\eta') = \frac{1 + b\eta'}{1 + \frac{2}{3}b}\,,\quad -1 < \eta < 0,\tag{15}$$

where b -- is the unknown parameter of angular distribution of ascending radiation which changes with altitude from 1 to 0. Substituting (14) in (11) we transform (10) to the form

$$J\!\uparrow(H,\eta,\lambda) = \omega \int_0^H \left[K_1 J\!\downarrow(H',\lambda) + K_2 J\!\uparrow(H',\lambda)\right] e^{-\frac{\alpha}{|\eta|}(H-H')}\,\frac{\alpha}{\eta}\,dH' +$$
$$+ J\!\downarrow(0,\lambda)\, A(\lambda)\, e^{-\frac{\alpha H}{|\eta|}},\tag{16}$$

where α-- is the coefficient of eccentrics, H -- is altitude in a uniform atmosphere and the values of K_1 and K_2 equal:

$$K_1 = \frac{1}{4\pi} \int_0^{2\pi} d\gamma' \int_0^1 u \, i(\eta) x(\gamma) \, d\eta', \qquad (17) \quad \underline{/8}$$

$$K_2 = \frac{1}{4\pi} \int_0^{2\pi} d\gamma' \int_{-1}^0 u \, i(\eta') x(\gamma) \, d\eta'. \qquad (18)$$

Using formulas (12), (13), (15) and `[- illegible -]`, we find that $K_1 = 0.46$; $K_2 = 0.53 \pm 0.08$. Transfering in equation (16) from intensities to average intensity W_{ij} according to (1) and using the relationship resulting from figures 4-7;

$$W_{1j}(H) = W_{1j}(0)(1 + C_j H) \qquad (19)$$

and

$$W_{3j}(H) = W_{1j}(0)(A + C_j H'), \qquad (20)$$

where C_j -- is the angular coefficient, we find:

$$W_{3j}(H) = W_{1j}(0) g(H, \eta_0) \frac{\omega \alpha_j}{|\eta_0|} \int_0^H [K_1(1 + C_j H) + K_2(A + C_j H)] e^{-\frac{\alpha_j}{|\eta_0|}(H - H')} dH' + W_{3j}(0) e^{-\frac{\alpha_j}{|\eta_0|}H}, \qquad (21)$$

where α_j -- is the average for the j spectral range of the coefficient of eccentrics;

$$\alpha_j = \frac{\int S_j(\lambda) J(\lambda) \alpha(\lambda) d\lambda}{\int S_j(\lambda) J(\lambda) d\lambda} ; \qquad (22)$$

$g(H, \eta 0)$ -- is the factor which takes into consideration the effect of the value of width of the beam pattern $F_{3j}(\eta)$:

6

$$g(H, \eta_0) = \frac{\int d\varphi \int_{-1}^{0} \Im\uparrow(\eta, H) F_{3j}(\eta, \varphi)\, d\eta}{\Im\uparrow(\eta_0, H) \cdot \int d\varphi \int_{-1}^{0} F_{3j}(\eta, \varphi)\, d\eta}. \tag{23}$$

The value $g(H, \eta_0)$ essentially increases the unit only when $|\eta_0| \mp 0.08$ and $\tau < 0.5$ reaching, for example, when $|\eta_0| = 0.65$ and $\tau = 0$, the value 1.25:

η_0 -- is the cosign of the angle of inclination of the axis of the beam pattern (optical axis) to the vertical.

Fulfilling integration in (21), we find the equation involving measured intensities W_{1j} with the coefficient of eccentric α_j and /9 inclination of the axis of the vehicle:

$$\frac{W_{3j}(H) - W_{3j}(0) e^{\frac{-\alpha_j H}{|\eta_0|}}}{W_{3j}(0)} = g(H, \eta_0)\, \omega x \cdot$$
$$x \left\{ \left(1 - e^{\frac{-\alpha_j H}{|\eta_0|}} \right) \left[\left(K_1 + K_2 A \right) - \frac{C_j |\eta_0|}{\alpha_j} (K_1 + K_2) \right] + C_j H (K_1 + K_2) \right\}. \tag{24}$$

The value of η_0 involves the angle ς between the axis of rotation and normal to the surface

$$\eta_0 = \cos\xi \cos\zeta - \sin\xi \sin\zeta \cos\psi, \tag{25}$$

where ψ-- is the angle of rotation of the vehicle, ξ-- is the angle between the axis of the vehicle and the optical axis.

Here, in order to determine the angle ς for the Venera-9 spacecraft, we will introduce the monotonic functions $W_{3j max}(H)$ and $W_{3j min}(H)$, whose graphs, pass, respectively, through the periodic maximums.

and minimums of curves $W_{3j}(H)$. For the function $W_{3j\max}(H)$ from formula (25) we find that $|\eta_0|=\cos(\zeta+\xi)$, and for $W_{3j\min}(H)$ we find that $|\eta_0|=\cos(\zeta-\xi)$. In a case where the axis of the vehicle is vertical, but the surface is sloped at an angle ζ to the horizon, the value of $|\eta_0|$ in formula (24) must be substituted for

$$\frac{|\eta_0|}{\cos\zeta} = \frac{\cos\xi\cos\zeta - \sin\xi\sin\zeta\cos\psi}{\cos\zeta} . \tag{26}$$

When $H\to 0$ from (24) with a calculation of (25) it follows:

$$\frac{W_{3j\max}(H) - W_{3j}(0)}{W_{3j}(0)} = g(0,\eta_0)\,\sigma_j\,\frac{H}{\cos(\zeta+\xi)}\left(K_1 + K_2 A - \frac{A}{g(0,\eta_0)\,\omega}\right), \tag{27}$$

where $\delta_j = \omega\alpha_j$ -- is the coefficient of scattering; because $|\zeta-\xi|\approx 0$ and $g[c,\cos(\zeta-\xi)]\approx 1$, then

$$\frac{W_{3j\min}(H) - W_{3j}(0)}{W_{3j}(0)} = \sigma_j\,\frac{H}{\cos(\zeta-\xi)}\left(K_1 + K_2 A - \frac{A}{\omega}\right), \tag{28}$$

$$\frac{W_{3j\max}(H) - W_{3j}(0)}{W_{3j\min}(H) - W_{3j}(0)} = g(0,\eta_0)\,\frac{\cos(\zeta-\xi)}{\cos(\zeta+\xi)} . \tag{29}$$

Approximation (29) can be used when calculating the slope of the surface only for an altitude from 0 to approximately 200 m. To determine the /10 angle ζ for the entire range of altitudes shown in figure 5, equation (24) was used. By using this for calculating the relationship of $W_{3j\max}(H)$ and $W_{3j\min}(H)$ the functions of the ratio $\dfrac{W_{3j\max}}{W_{3j\min}}$ were constructed from altitude H and angle ζ with a given coefficient of eccentrics coinciding

8

with the Rayleigh. The results of calculation were compared with the experimental relationship of the ratio to altitude indicated. The best coincidence corresponds to the angle between the axis of the vehicle and normal to the surface equal to 25 $\pm$ 5°. The absence of separate measurements from the averaged value reaches 10°, which, besides measurement error, can be explained by the fact that the surface is not ideally flat.

If one assumes that the axis of the vehicle was vertical, we conclude that the Venera-9 space station sat at a steep slope of about 25°. The extent of the slope found according to time during which the variable component of ascending radiation flux was recorded is at least 3 km.

The coefficient of scattering σ was defined according to the value of slope of curves $W_{ij}(H)$ with large thicknesses ($H \approx 2.5$ km). Then, it is possible to consider that the ratio of the derivative $C_{ij} = dW_{ij}/dH$ to the value of $W_{ij}(0)$, that is, the value of intensity of radiation which reaches the surface, equals 0.68σ[3]. The value found this way of the coefficient of scattering is presented in the table in column 8.

In the table [illegible] , column 7, also values of the coefficient of scattering σ_p are found for a purely gaseous atmosphere of CO_2, calculated according to formula (22) and then $\sigma(\lambda)$ equals

$$\sigma_p(\lambda) = \frac{8}{3}\pi^3 \frac{(m^2-1)^2}{n_L} \frac{f}{\lambda^4} \frac{\rho'}{\rho_0} = \alpha(\lambda), \tag{30}$$

where n_L is the Loshmit number, $2.687 \cdot 10^{25}$ m^3-- is the index of refraction of CO_2, m -- 1=$4.5 \cdot 10^{-4}$[5], ρ_0 -- is density of CO_2 under

normal conditions, 1.997 kg/m^3 [5], ρ-- is density at the surface of

Venus, f-- is the factor of depolarization.

The density on the surface of the planet was determined according

to the model of the atmosphere [6] using data on pressure on the sur-

face in the landing areas of the Venera-9 and Venera-10 [7]. It

appeared to be equal to 59.3 kg/m^3 and 62.7 kg/m^3 for the Venera-9

and Venera-10 spacecraft, respectively. The values of the factor of

depolarization of CO_2 presented by different authors, differ from each

other somewhat, f=1.103 8 and f=1.17 9 . When calculating at the value

$\delta_p(\lambda)(30)$ the value f from {9} was used. A certain indeterminancy in

the value of the factor of depolarization, the error of experimental

determination of ρ and noncalculation of nonideal gas and relationships

of the index of refraction m to the wavelength result in the following

error in calculating the value $\sigma_j : \frac{\Delta \sigma_j}{\sigma_j} = \pm\, 0.07$.

In the table, column 9, the ratios of theoretical and measured values

of the coefficients of scattering are presented. By analyzing these

results, it is possible to say that the coefficient of scattering in

the near-surface layer of the atmosphere of Venus coincides with the

Rayleigh for all CO_2 within the limits of $\frac{10\%}{25\%}$. The difference be-

tween measured and calculated coefficients of scattering can be

explained by errors in calculation and measurement.

3. Albedo of the Surface.

For calculating the albedo of the surface depending on wavelength

$A(\lambda)$ the results of measurements of intensity $W_{[illegible]j}$ extrapolated

at the moment of landing and obtained in the last few seconds before

landing of the Venera-10 and Venera-10 spacecraft were used. The

albedo of the ground with a wavelength $\overline{\lambda}_j$ was defined as the ratio

10

$\frac{W_{3j}(0)}{W_{1j}(0)}$, and the first standardized moments of the function $S_j(\lambda)$ was used as $\overline{\lambda}_j$. The results obtained are presented in figure 8.

In the graphs of figure 8 one notes possible deviations of the values $A(\overline{\lambda}_j)$ caused by measurement error which we evaluated as 25 -- 30%. Error comes from the following: a) calibration of the instrument, b) calculation of instability characteristics of the instrument, c) calculation of the effect of the parts of the spacecraft found in /12 the field of vision of the instrument, d) corrections on resulted calibration of the instrument during landing, e) processing of results of measurement, f) those involving the discreet nature of telemetry. The values obtained of the albedo A characterize sections of the surface with dimensions 10-30 m. The values found of A are closer to a flat albedo, that is, to the ratio of radiation flux from the lower hemisphere to flux from the upper hemisphere. With an orthotropic indicatrix of reflection of the ground, these two values coincide.

Photometric processing of the panorama of the surface [10] indicated that the indicatrix of reflection actually is close to the orthotropic. At the maximum, completely improbable case, reflecting indicatrices or indicatrices with a strong back scattering (lunar type), the value of A is smaller than the flat albedo by 30%.

Independently, evaluations of the albedo of the surface were made with photometric processing of the panorama [10]. A method of comparison of brightness of characteristic sections of the surface with brightness of the calibrated standard was used. The calibrated standard was the indicator of coloration of the landing platform with a known coefficient of reflection. In as much as in [10] there are no indications which could prove the shading of the standard of the surface

by the vehicle, in tne value of the albedo presented in [10] we intro-
duced a correction equal to 0.5. The correction was obtained according
to the data presented in figures 9 and 10. The values of the albedo
of characteristic sections of the surface obtained when processing the
panorama, taking into account the corrections, are presented in figure 8.
The wavelength in which we incorporated the value of the albedo from
[10], is the first standardized moment of spectral characteristics
of the telephotometer presented in [11]. As is seen from figure 8,
the data of work [10] agrees with the results of our measurements.
We note that the telephotometer and the broadband photometer are
located on diametrically opposite sides of the spacecraft.

The studies 12-15 showed that data on the value and spectral /13
distribution of the albedo of the ground, in principle, make it
possible to qualitatively evaluate the composition and characteristic
dimensions of the particles of soil. The authors of [12-15] studied
a large number of samples of different rocks for which a relationship
of the spectral albedo to the dimensions of the particles, their
shape, type of packing and conditions of illumination were obtained.
The authors of [15] studied 22 samples of volcanic rock and minerals
in order to present a full range of their characteristics (composition,
mineral content, origin and dimension of particles). In reference
[14] approximately 50 samples of rocks and minerals were studied.
We compared the relationships which we obtained of $A(\lambda)$ with the
spectra of Earth igneous rock presented in works [12-17]. The
petrographic description of the rocks studied is presented in [14].
The relief of the surface has a strong effect on the value of the
albedo. Any depressions result in a decrease in the albedo. This

12

effect, apparently, basically is responsible for the smaller value of the albedo of the ground in the landing area of the Venera-9 spacecraft in comparison with the albedo according to the data of the Venera-10. During a comparison with the spectra of reflection of Earth rock, we used data on the albedo of the ground for the landing area of the Venera-10 spacecraft where the effect of relief on the value of the albedo apparently is insignificant.

We will introduce the index of light $M=A(0.87)/A(0.54)$, that is, the ratio of the albedo of the graph with wavelengths 0.87 and 0.54 microns. The value of M according to the concept is close to the parameter R/B presented in [14] equal to $A(0.7)/A(0.4)$. In the work [14] it was pointed out that with identified rocks and an evaluation of the degree of its dispersion by certain characteristics, they are: parameter R/B, the value of the albedo and the position of the absorption band, and then these characteristics essentially differ for three groups of silicate rock. These are volcanic glass (obsidian /14 pumice), oxidized rock (tufa, rhyolite, granite), basic and ultrabasic rock (basalt, gabbro). The albedo of all identified rocks, after certain critical dimension d_{lc} begins to increase with an increase in the dimensions of the particles.

Taking into account the measurement error, parameter M for the ground of Venus = 2-7. A comparison of the parameter M with the data of [14] indicates the following. Volcanic glass and acid rocks can, apparently, be excluded from consideration: for the first R/B < 1.3; for the second, although 1.2 < R/B < 2.4, but $A(0.55) \geq 0.2$. From the base rocks, basalt (Pisgah)

satisfies our measurement according to the value of A and M for small particles d 53 micro m. For this, [illegible] less than R/B 2.5; $0.04 < A_{0.55} < 0.15$. It satisfies measurement [illegible] basalt (Red Cinder). The spectral albedo of certain rocks and minerals, which do not contradict the results of measurement are presented in figure 11.

In work [16] the reflective properties of basalt were studied depending on the degree of their oxidation. It appears that the higher the degree of oxidation the smaller is the coefficient of reflection in the short wave field of the spectrum and the better than relationship $A(\lambda)$ for it coincides with our measurements (figure 12). We note that CO_2 oxidizes basalt [18]. Only basalt of the Earth igneous rocks can satisfy the albedo of the ground of Venus measured; this agrees with the data of [19,20].

Although the values of A and M for the ground of Venus and certain types of basalts coincide, the character of the relationship of $A(\lambda)$ in them is different (figures 11, 12). When evaluating the composition of Martian rock according to the spectrum of their reflection, it was established that the albedo of the ground of Mars satisfies well a mixture of different rocks, for example, basalt plus geothite; basalt plus limonite [16,21]. Apparently, the albedo of the ground of Venus can agree only with the coefficient of reflection of a mixture of different rocks. In our opinion, mixtures of basalts with a different /15 degree of oxidation with the addition of geothite or limonite are promising.

4. Dust on the Surface.

Immediately after landing of both spacecraft, a sharp decrease in radiation from below was established and a certain much smaller decrease in radiation from above. This phenomenon can be explained by the shading of the ground by the spacecraft components because after a few seconds radiation again increases and goes to a certain stationary level. This level is below that which was obtained by extrapolation at the moment of landing in data obtained during descent; this is explained by the shading mentioned above. In figures 9 and 10, the ratio of readings of the instrument to readings at the moment of landing depending on time are shown and calculation of time is done from the moment of landing. In this way, at the moment of landing at a certain time, a factor occurs which decreases radiation from below. Then this factor disappears. This is all usually explained if one assumes that the instrument fixes the dust cloud at the moment of landing.

In motion, the spacecraft vehicle every second transmits in the atmosphere of Venus the quantity of motion mg_B where m is the mass of the spacecraft, g_B -- is the acceleration of the force of gravity on Venus.

As a result, a turbulent path of the spacecraft is formed, that is a column of gas entrapped by the vehicle. The diameter of the path B increases as one gets farther from the spacecraft and the velocity of the gas U in the path directed downward disappears, tending toward 0 for an infinite distance X from the spacecraft. Assuming an idealized point for the spacecraft in which the quantity of motion in the atmosphere is transmitted, we find an evaluation

15

[22] for B and U depending on the distance X:

$$B \simeq \left(\beta \cdot C_x \cdot S \cdot X \right)^{1/3}, \qquad (31)$$

$$\frac{U}{U_{sc}} = \left(\frac{C_x \cdot S}{\beta^2 \cdot X^2} \right)^{1/3}, \qquad (32) \quad /\underline{16}$$

where β is a constant which characterizes turbulent exchange ($\beta \simeq 0.2$), U_{sc} -- is the rate of descent of the spacecraft, C_x -- is the coefficient of resistance of the spacecraft (approximately 0.91), S -- is the area [illegible] of the spacecraft. Estimates (31) and (32) are true for an adequate distance from the spacecraft when $(X/\sqrt{S}) > 50$. Figure 13 shows the results of calculations of B and $\frac{U}{U_{sc}}$ according to formulas (31) and (32).

It is apparent that even at a distance of 100 m from the spacecraft, a significant velocity directed downward of the gas in the path is retained. At the landing moment the spacecraft is stopped but the gas in the path continues to move downward coming in on the spacecraft and the surface of the planet (figure 14,a,b). With this flow of gas, it is capable of raising a cloud of dust. It is characteristic that at first the dust over the vehicle cannot appear because it is blown away by the track (figure 14 c). At this moment under the shield of the vehicle a zone of eddy flow occurs in which the dust is raised and maintained gradually settling. In the graph of figure 10 (curves $W_{3j}(t)$) a sharp drop at the moment $t \simeq 0$ is visible. Then, on the graphs, a smooth rise in the curve is visible involving settling and drifting of the particles from the wind. Figure 15 shows the calculation velocities of settling of spherical particles on the

surface of Venus depending on their diameter. It is apparent that with the characteristic velocity of gas in the cloud of approximately 1 m/s, particles are found in it with a diameter d≤1 mm. The process of attenuation of the track (all of the more distant parts of the track move toward the spacecraft at ever decreasing velocity) is accompanied by drift of the track in the wind. For 10 seconds the track as a whole is shifted by the wind for 5-10 m from the spacecraft and actually interacts with it. As the track moves it becomes possible for the cloud of dust to drift under the spacecraft (figure 14, d,e). This results in failure in the readings of the 2j and 1j channels. For evaluating the time of this shift, the data [23] on wind velocity at an altitude /17 of H≈1 m were extrapolated for the layers lying above (H<10 m). It was assumed that the profile of wind velocity $U_b(H)$ has, like the ground layer, a logarithmic character.

$$\frac{U_\varepsilon(H_1)}{U_\varepsilon(H_2)} = \frac{\lg(H_1/z_0)}{\lg(H_2/z_0)} ,$$

(33)

H_1 and H_2 are certain altitudes and the value Z_0 at a Reynolds number $Re >> 10^4$ involves only the height of roughness of the surface and approximately can be assumed as 0.1 d_k where $d_k \approx 0.3$m -- the average diameter of rocks visible on the panorama. Figure 16 shows the results of extrapolation of velocity U_b at an altitude of H≈1 m for layer $Z_0 \leq H \leq 10$ m according to formula (33). An insignificant change in wind velocity in the 10 meter layer over the spacecraft and rapid attenuation of wind velocity when H<1 m, that is, under the spacecraft, is common

for all profiles. (during calculation, the effect of the spacecraft itself on distribution was not considered). In this way, the mean wind velocities in the 10-meter layer directly over the vehicle must be 0.5 and 0.1 m/s for the Venera-9 and Venera-10, respectively, and the time of drift of the 10-meter cloud of dust is 10s which corresponds to experimental data for the Venera-10 spacecraft.

We will use the data on change of W_{3j} for evaluating the quantity of dust raised per unit of volume under the shield of the spacecraft. From the very beginning it is clear that very rough evaluations can be presented here because the configuration of the dust cloud is not known, nor the distribution of particles according to dimensions as well as many other factors. In view of this, the problem was simplified as much as possible and the following hypotheses were introduced.

1. In the field of vision of the instrument (channels 3j) which is a cone, suspended particles of dust were found. The radiation perceived by the instrument consists of radiation scattered by these particles and radiation scattered by the particles of the ground /18 in the field of vision.

2. The particles are spheres of uniform diameter d.

3. The particles are large in comparison with the wavelength of radiation.

4. Their surface is scattered according to the Lambert law and in this way the indicatrix of scattering of particles is: $x(\gamma)-\sin\gamma+(\pi-\gamma)\cos\gamma$.

5. The coefficient of reflection of the surface of the particles is less than 0.2, that is, it can be limited only to consideration of a single scattering.

18

6. The cloud of dust has the shape of a truncated cone and from above is limited by the shield; the angle at the apex of the cone is 40°.

Hypothesis 5 can be supported in the following way. With velocities of flow approximately 1m/s, particles with dimensions ≤ 10⁻³m can be lifted. These large particles are opaque, and the coefficient of their reflection is close to the coefficient of reflection of monolithic rock. For example, for basalt, the characteristic value of the albedo is 0.1 and the coefficient of absorption lies in the range from $2 \cdot 10^4$ to 10^5 1/m. Thus, when d > 10 μm the basalt particles are not transparent. The presence of finer particles on the surface would be shown by the presence of local light sections on the panoramas because these particles must fill the small irregularities of the surface and then form fairly smooth sections. Thus, the hypothesis is proven that d>10 μm and the coefficient of reflection of the surface of the particles is close to the coefficient of reflection of the lighter sections of the surface, that is, approximately 0.1. Let us consider the spherical layer with thickness dy obtained by intersection of the cone (beam pattern of the instrument) by two spherical surfaces with the center at the apex of the cone and radii y and y+dy (figure 17). The quantity of particles in this layer equals $N\Omega y^2 dy$, where Ω is the solid angle limited by the beam pattern, N -- is the quantity of particles per unit of volume. The flow of the dy layer of radiation scattered into particles received by the instrument amounts to:

$$dL = a \cdot X E \cdot N \cdot \frac{\pi d^2}{4} \varepsilon^{-N \frac{\pi d^2}{4} y} \cdot dy, \tag{34}$$

19

where a -- is the coefficient of reflection of the surface of the particle, E -- is irradiance, y-- is the multiplier involved with the indicatrix of scattering of the particles, $e^{-N\frac{d^2}{4}}$ y is the multiplier taking into account absorption of dust of the scattered radiation. Designating $=N \cdot \frac{d^2}{4}$, we find

$$F = a \cdot \chi \cdot E' \int_0^{\sigma y_0} e^{-\sigma y} \cdot dy =$$

$$= a \cdot \chi E' \cdot (1 - e^{-\sigma y_0}) \qquad (35)$$

the flux recorded by the instrument of radiation scattered by particles. (y_0 -- is the distance from the receiving end of the light guide to the ground).

Weakening or radiation K on the path from the boundary of the dust cloud to the axis of the field of vision taking into account its geometric dimension equals:

$$K = \frac{1}{0,5\sigma} \cdot e^{-0,95\sigma} \cdot (e^{0,5\sigma} - I) \cdot 0,3 \ . \qquad (36)$$

With the absence of dust recorded before landing, the radiation flux below F_Γ is defined as scattering on the section of ground in the field of vision of the instrument:

$$F_\Gamma = A \cdot E_\Gamma$$

(A and E_Γ -- is the coefficient of reflection of the ground and irradiance of the ground). F_Γ corresponds to extrapolation of results with flying up at the moment of landing.

Calculation of the effect of the spacecraft after landing on the readings of the instrument leads to definition of the factor of shading K_3 of the section of ground by parts of the spacecraft visible

by the instrument. $K_3 \approx 0.5$. Moreover, before reaching the ground, the light passes through the dust cloud which is taken into account by the multiplier K . Similarly to (36):

$$K_\Gamma = \frac{I}{0.5\sigma} \cdot e^{-0.95\sigma} (e^{0.5\sigma} - I) \cdot K_3 \quad . \tag{37}$$

Moreover, weakening of the flux of radiation reflected from the ground /20 occurs in the cloud of dust before it reaches the instrument. Thus, after landing:

$$F_r' = A \cdot E_r \cdot K_r \cdot e^{-\sigma y_o} \quad .$$

The ratio of the total flux scattered from the dust particles and ground F_Σ to F_Γ , shows with calculation that ax $\approx$ A and $y_o \approx$ 1 m:

$$\frac{F_\Sigma}{F_r} = \left[0.5\, e^{-\sigma} + 0.3(1 - e^{-\sigma}) \right] \cdot \frac{1}{0.5\,\sigma}\, e^{-0.95\sigma} \cdot \left(e^{0.5\sigma} - 1 \right) \quad . \tag{38}$$

Taking into account that in the experiment $F_\varepsilon/F_\Gamma = 0.15$ and 0.2 (for the Venera-9 and Venera-10, respectively) we find:

$$\sigma = I.3 \div 0.9 \left(\frac{I}{M} \right) = N \cdot \frac{\pi d^2}{4} \quad .$$

The volume content of dust in the cloud with a density of dust particles $2.8 \cdot 10^3 \text{kg/m}^3$ is shown to equal 10^{-1} -- 10^{-2} kg/m^3 for diameters of the dust particles 0.1 -- 0.01 mm, respectively. If one considers that the cloud has a hemispheric shape with a radius of 1 m, and the dust in the cloud is raised from the area of a surface limited to this hemisphere, then [illegible] thickness of the layer of dust on the surface amounts to 10^{-1} -- 10^{-2} mm for diameters of the dust

21

particles 10^{-1} -- 10^{-2} mm. The specific mass of the dust amounts to 10^{-1} -- 10^{-2} kg/m^2.

Generally one should note that recorded velocities of wind of 0.5 -- 1 m/s at an altitude of 1 m are adequate to judge all the dust with a dimension less than 1 mm. One can assume that the dust is accumulated in depressions between rocks where it is protected from the direct effect of horizontal wind. However, these depressions cannot be an effective protection from strong vertical perturbation in the atmosphere caused by landing of the spacecraft.

Conclusions

Characteristics of the field of radiation in the near-surface layer of the atmosphere and on the surface of Venus are determined experimentally. Interpretations of these data make it possible to obtain a good deal of information on the characteristics of the surface of the planet: It is found that the section of the surface with dimensions in tens of meters has practically the same optical characteristics as the surface of the landing point. This makes it possible to conclude that local characteristics of the ground obtained after landing by other instruments can be distributed on a broader section than that considered above.

/21

The presence of free dust on the surface was detected experimentally for the first time which makes it possible to look again at the process of interaction of the atmosphere with the surface of the planet.

Independently the instrument detected rotation of the vehicle during descent and determined at high altitudes the presence of a slope of a significant section of the surface.

The relationship of the albedo of the ground of Venus to wavelength was obtained for the first time; this made it possible to compare the surface rocks of Venus with those on Earth.

All of this indicates large possibilities for an optical method of studying the atmosphere and surface of planets using spacecraft. The authors wish to thank V. M. Pokras, L. V. Yabrova, E.B. Shesterkova, Z. V. Ivanova, S. T. Lukovinkova and many others who have given considerable help in completion of this work.

Table
Initial Data and Results of Calculation of the Coefficient of Scattering

1	2	3	4	5	6	7	8	9	10
	j	λ_{ef}, μm	C_{1j} км$^{-1}$	C_{3j} км$^{-1}$	C_ρ км$^{-1}$	σ_ρ км$^{-1}$	σ_{ms} км$^{-1}$	$\dfrac{\sigma_\rho}{\sigma_{ms}}$	ξ
Venera-9	1	0,535	0,65	0,61	0,63	1,07	0,925	1,16	30
	2	0,6	0,38	0,37	0,375	0,675	0,55	1,23	20
	3	0,67	0,31	0,22	0,265	0,435	0,39	1,12	23
	4	0,72	0,18	0,18	0,18	0,325	0,265	1,22	18
	5	0,775	0,16	0,13	0,145	0,243	0,213	1,14	23
Venera-10	1	0,535	0,77	0,74	0,755	1,13	1,11	1,02	15
	2	0,6	0,44	0,43	0,435	0,71	0,64	1,11	23
	3	0,67	0,38	0,28	0,33	0,46	0,485	0,95	23
	4	0,72	0,25	0,26	0,255	0,345	0,375	0,92	27
	5	0,775	0,2	0,18	0,19	0,257	0,28	0,92	15

Symbols:

j -- Number of the spectral range.

λ_{ef} -- The effective wavelength, which according to (30) corresponds to the value $\sigma(\lambda_{ef}) = \delta_{cal}$.

C_{1j}^{j} and C_{3j} -- Angular coefficients of the relationships of $W_{1j}(H)/W_{1j}(0)$ and $W_j(H)/W_{1j}(0)$.

σ_{cal} -- Coefficient of Rayleigh scattering, calculated according to formulas (22) and (30).

σ_{ms} -- Coefficient of scattering found from experimental data.

ξ -- The angle between the axis of the vehicle and the optical axis.

24

Subscripts for the Figures

Fig. 1. Spectral characteristics of a photometer.

Fig. 2. Beam patterns of a photometer. -- the angle of slope of the optical axis of channels 3j. For comparison a cosinusoidal beam pattern is constructed.

Fig. 3. The intensity of radiation incident on the surface averaged for the upper hemisphere.

Fig. 4. The relationship of average intensity of incident radiation W_{1j} to altitude in the uniform atmosphere A and to time before landing t; Venera-9.

Fig. 5. The relationship of average intensities of ascending radiation W_{3j} to altitude in a uniform atmosphere H and to time before landing t; Venera-9.

Fig. 6 The relationship of average intensity of incident radiation W_{1j} to altitude in a uniform atmosphere H and to time before landing t; Venera-10.

Fig. 7 The relationship of average intensities of ascending radiation W_{3j} to altitude in a uniform atmosphere H and to time before landing t; Venera-10.

Fig. 8 Relationship of the albedo of the ground to wavelength. The albedo of characteristic sections on the panorama 10 : 1 -- rock 12, Venera-10; 2 --plate 4, Venera-10; 3 -- about sections 10, Venera-10; 4 -- rock 3, Venera-9; 5 -- crushed rock 9, Venera-9.

Fig. 9 Results of measurement of radiation from above in the landing process.

Fig. 10 Results of measurement of radiation from below in the landing process.

Fig. 11 A comparison of the measured spectral albedo of the ground of Venus with coefficients of reflection of the Earth igneous rock: 1,2 -- albedo of the ground in landing areas of the Venera-9 and Venera-10 spacecraft; 3 -- hornblende, d=420 500 µm [15] ; 4 -- biotite d=420-500 µm [15] ; 5 -- nonpolarized limonite [17]; 6 -- basalt (Red Cinder) [14].

Fig. 12. A comparison of the measured spectral albedo of the Venus ground with a coefficient of reflection of Earth igneous rock: 1 -- albedo of the ground in the landing area of the Venera-10; 2 -- basalt (Little Lake), d=74-104 μm depending on the degree of oxidation [16]; 3 -- oxidized basalt (Little Lake), =147-246 μm [16]; 4 -- powder d=74-104 μm: 98% basalt (Little Lake) +2% geothite [16]; 5 -- powder d=74-104 μm: 94 % basalt (Little Lake) +6% geothite [16].

Fig. 13 An evaluation of the parameters of the turbulent layer behind the spacecraft.

Fig. 14. Phases of formation of a dust cloud.

Fig. 15. Rate of settling of spherical particles on the surface of Venus.

Fig. 16. Calculated profiles of wind velocity in the near-surface layer.

Fig. 17. Scattering and attentuation of light in a dust cloud.
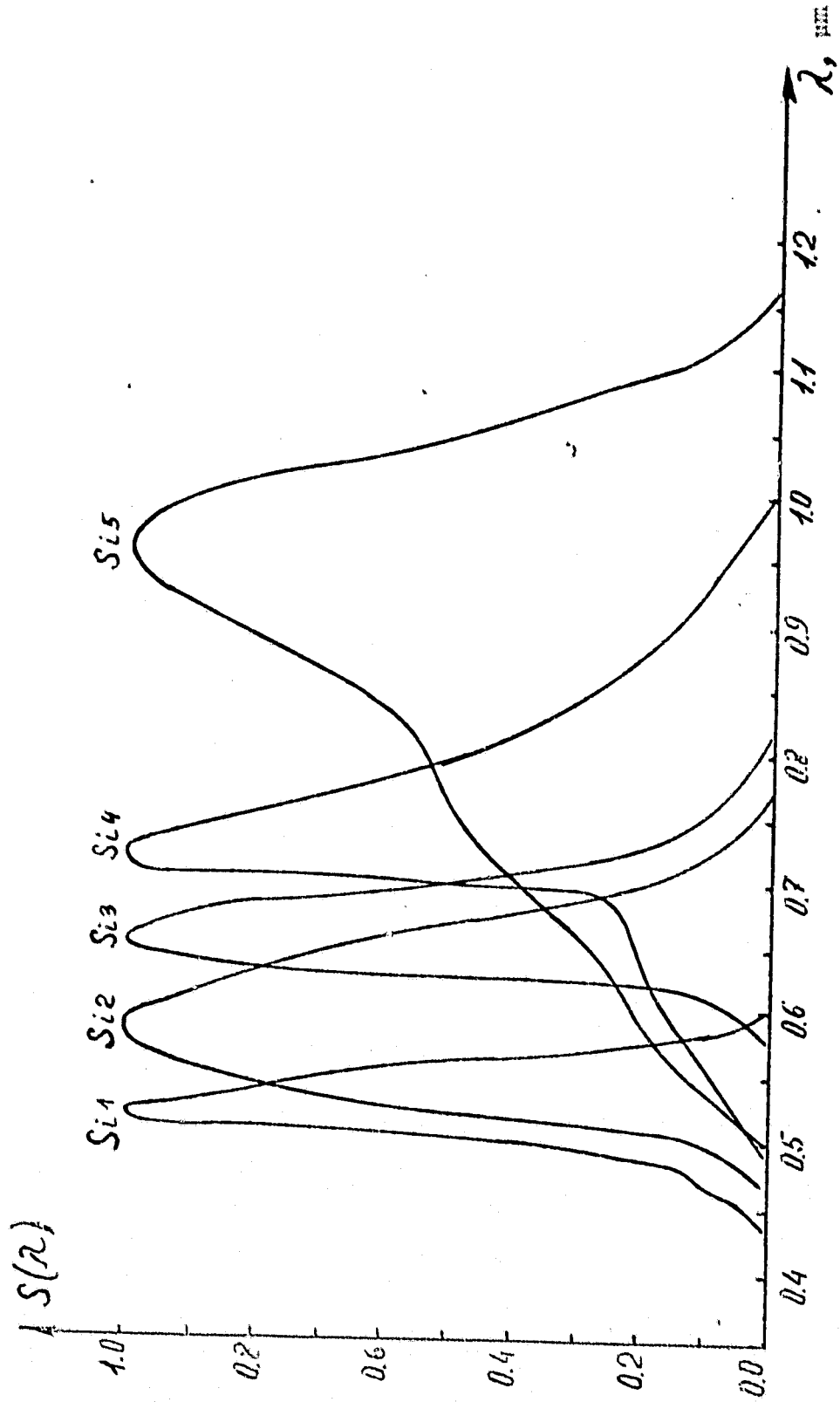
Figure 1
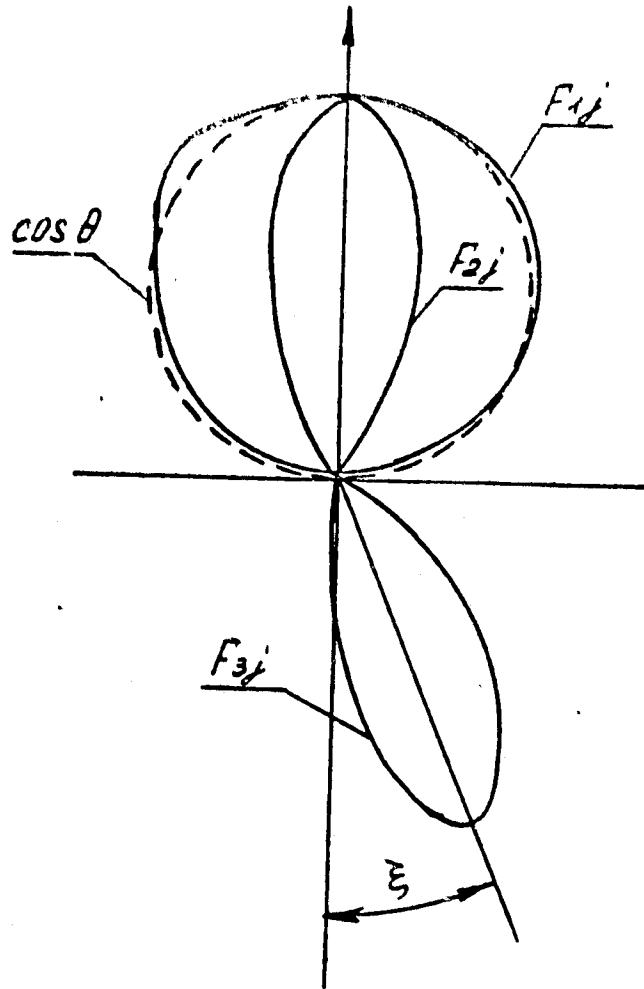
Figure 2
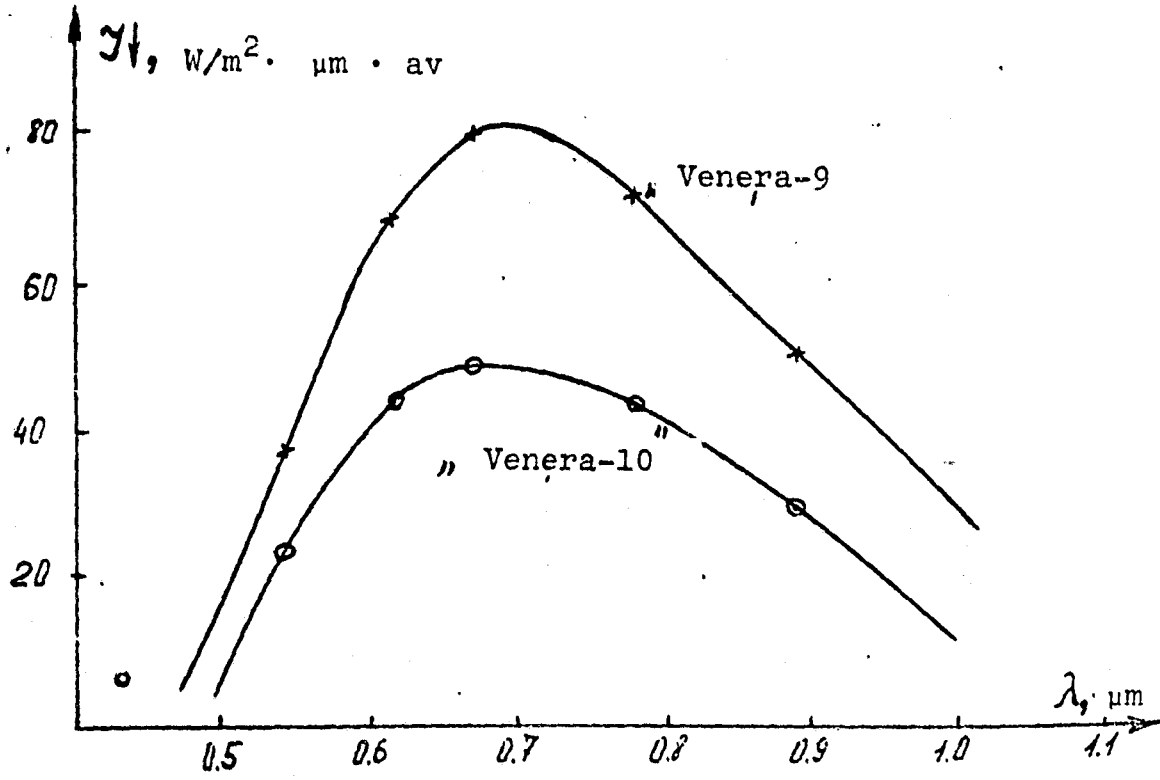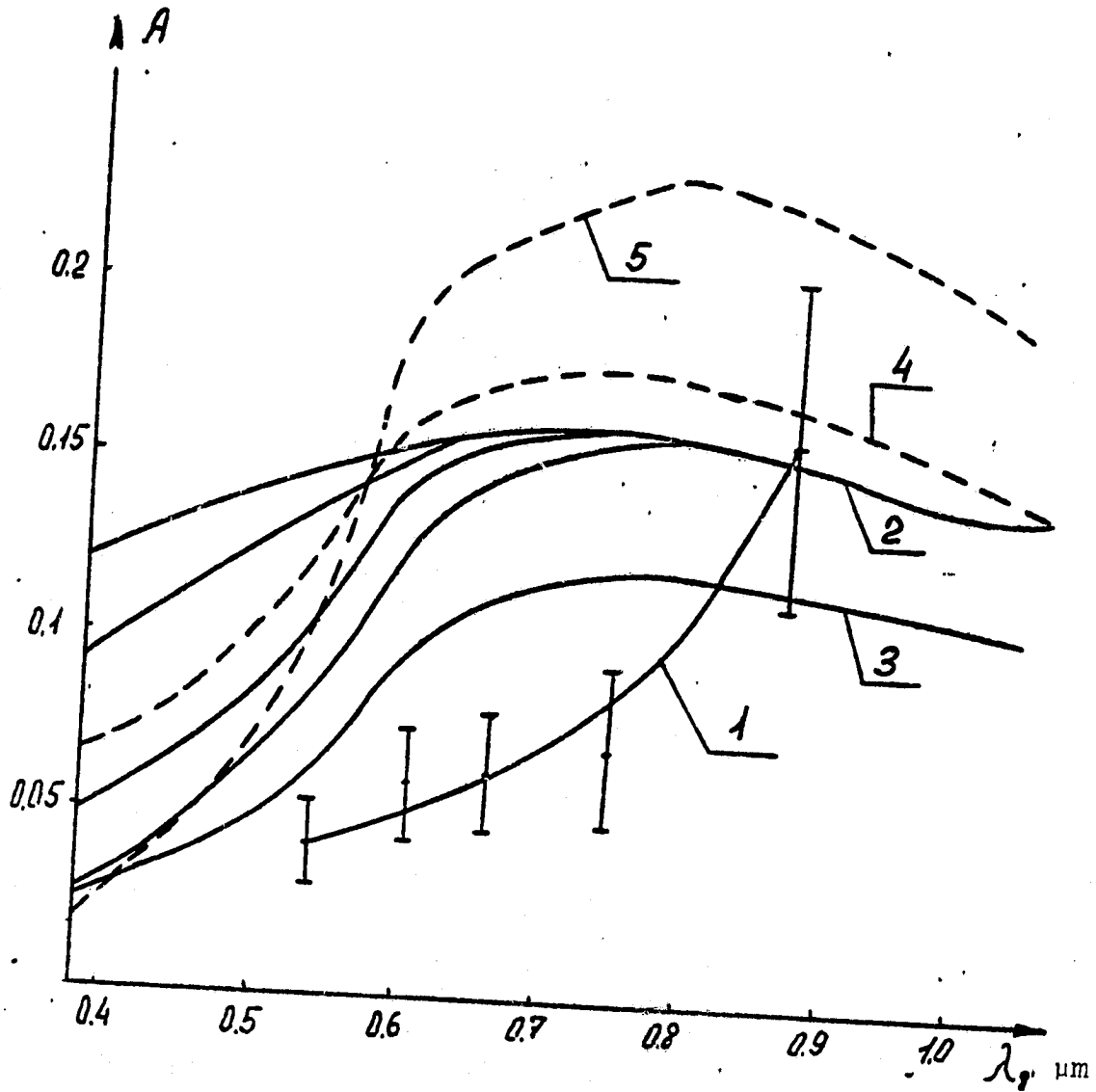
Figure 3
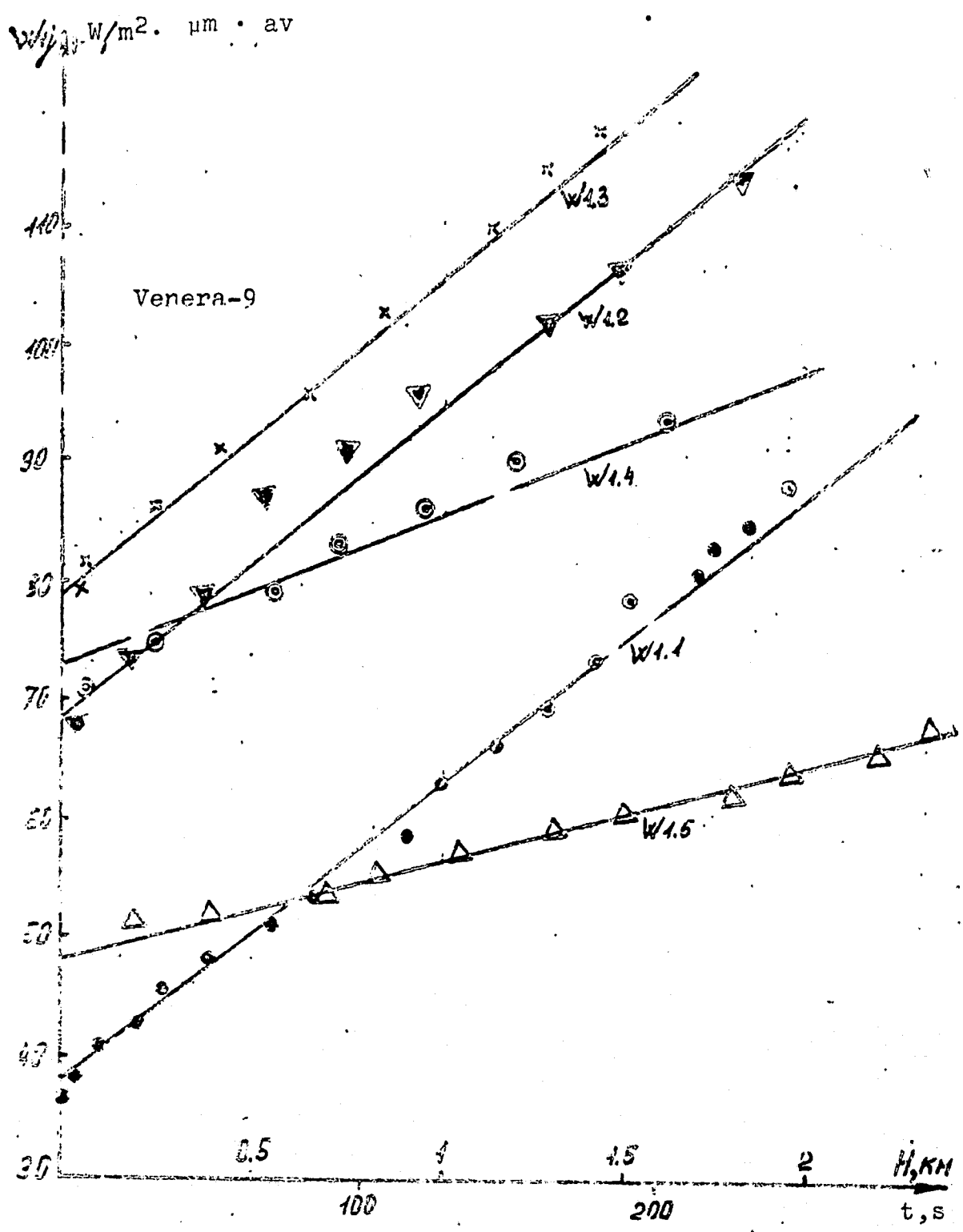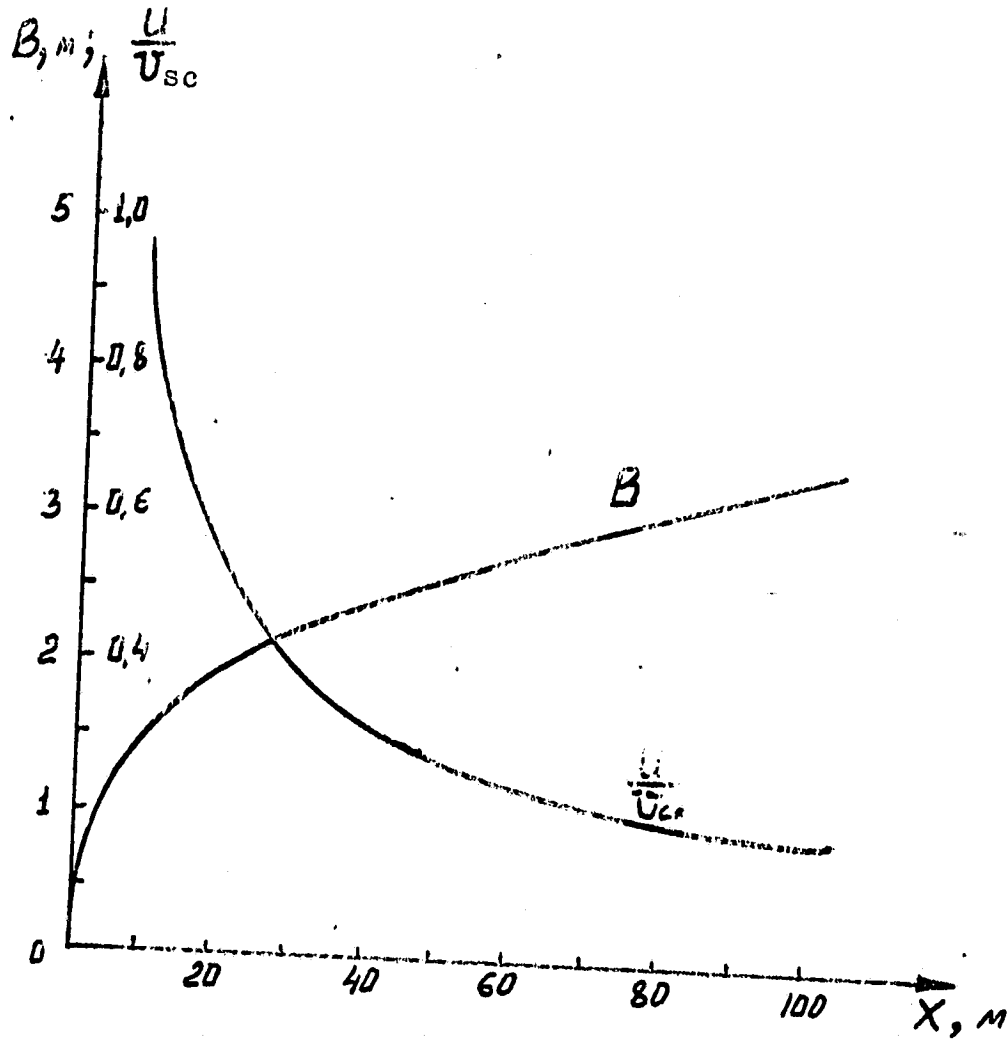
Figure 4
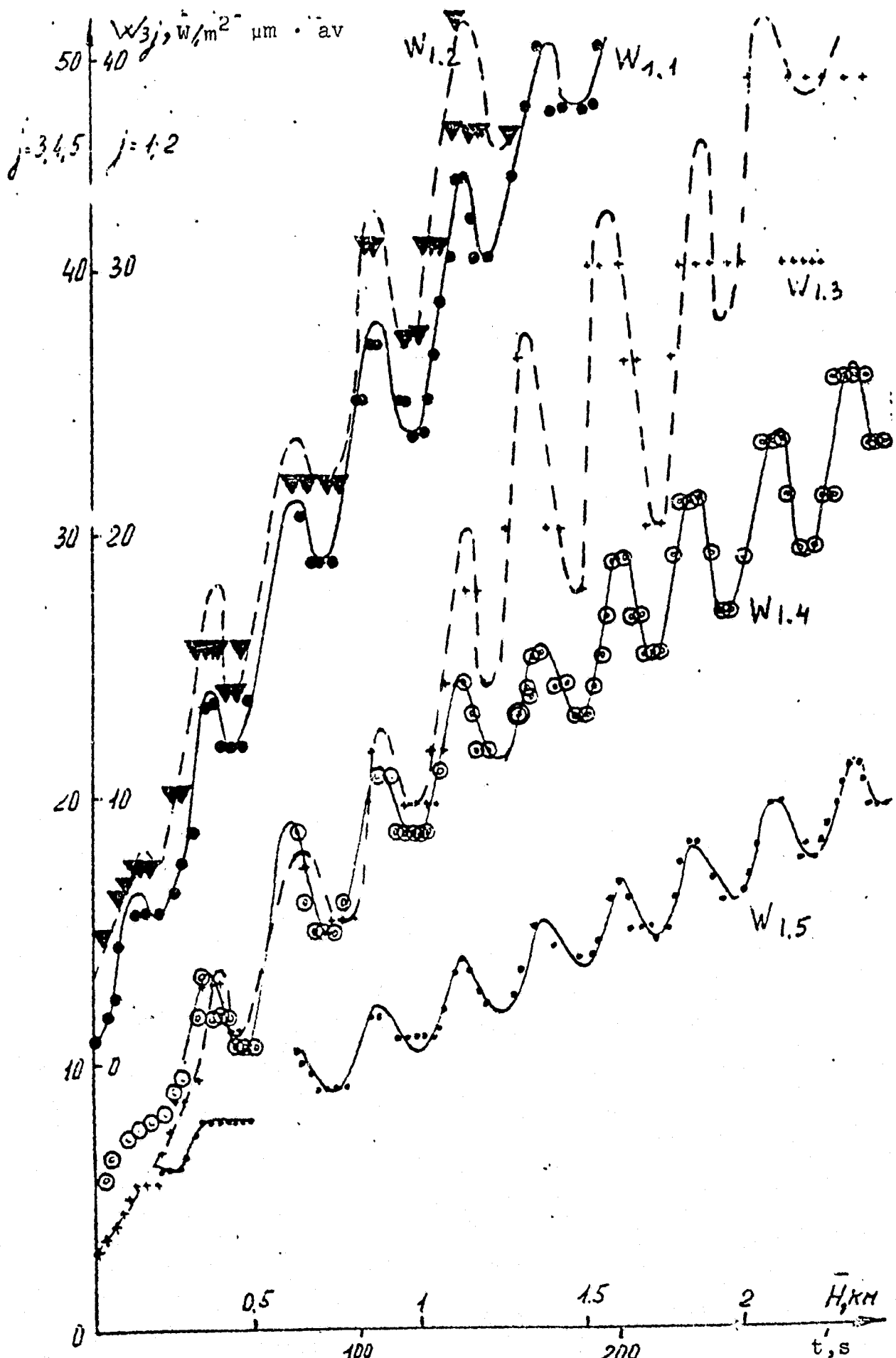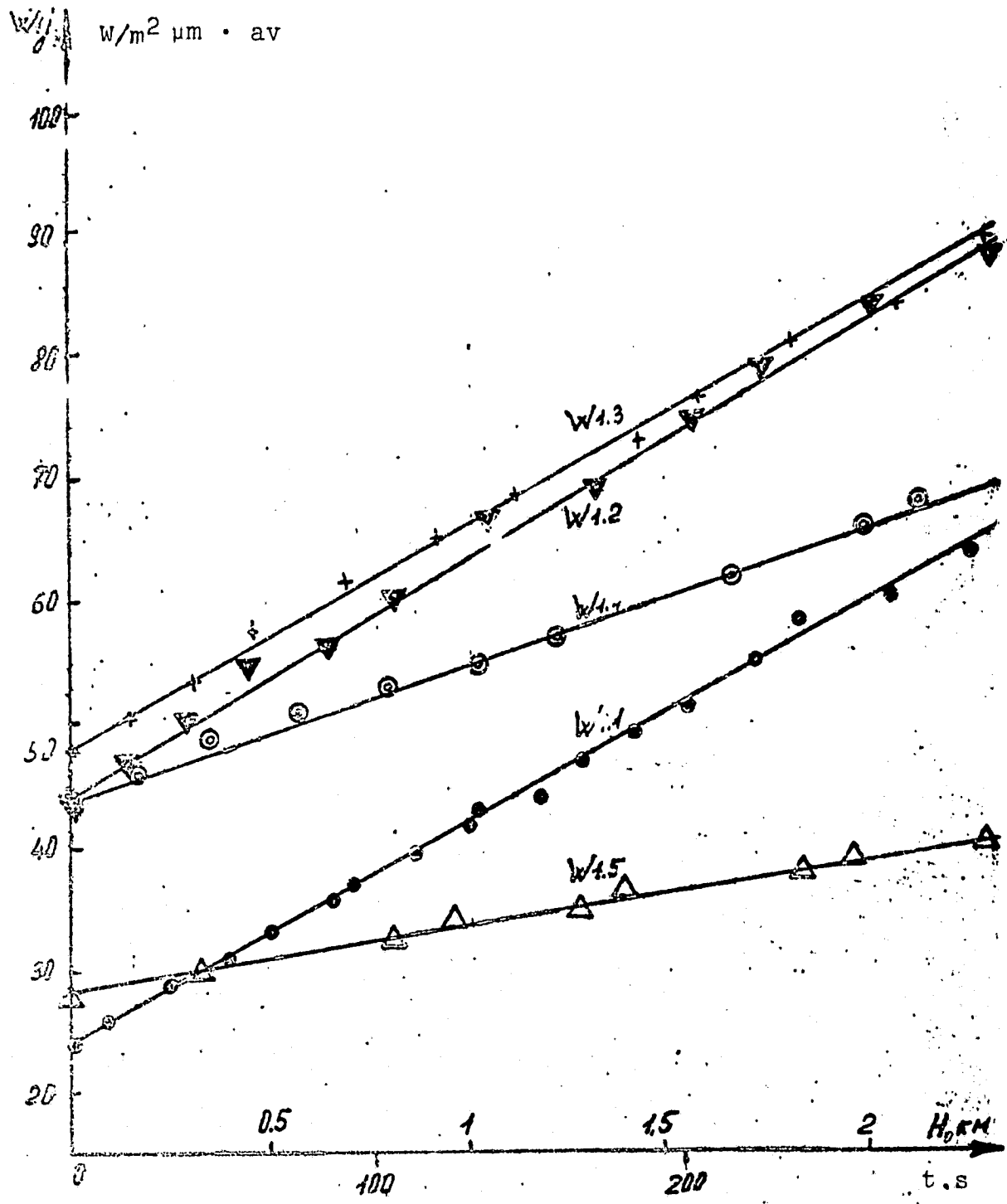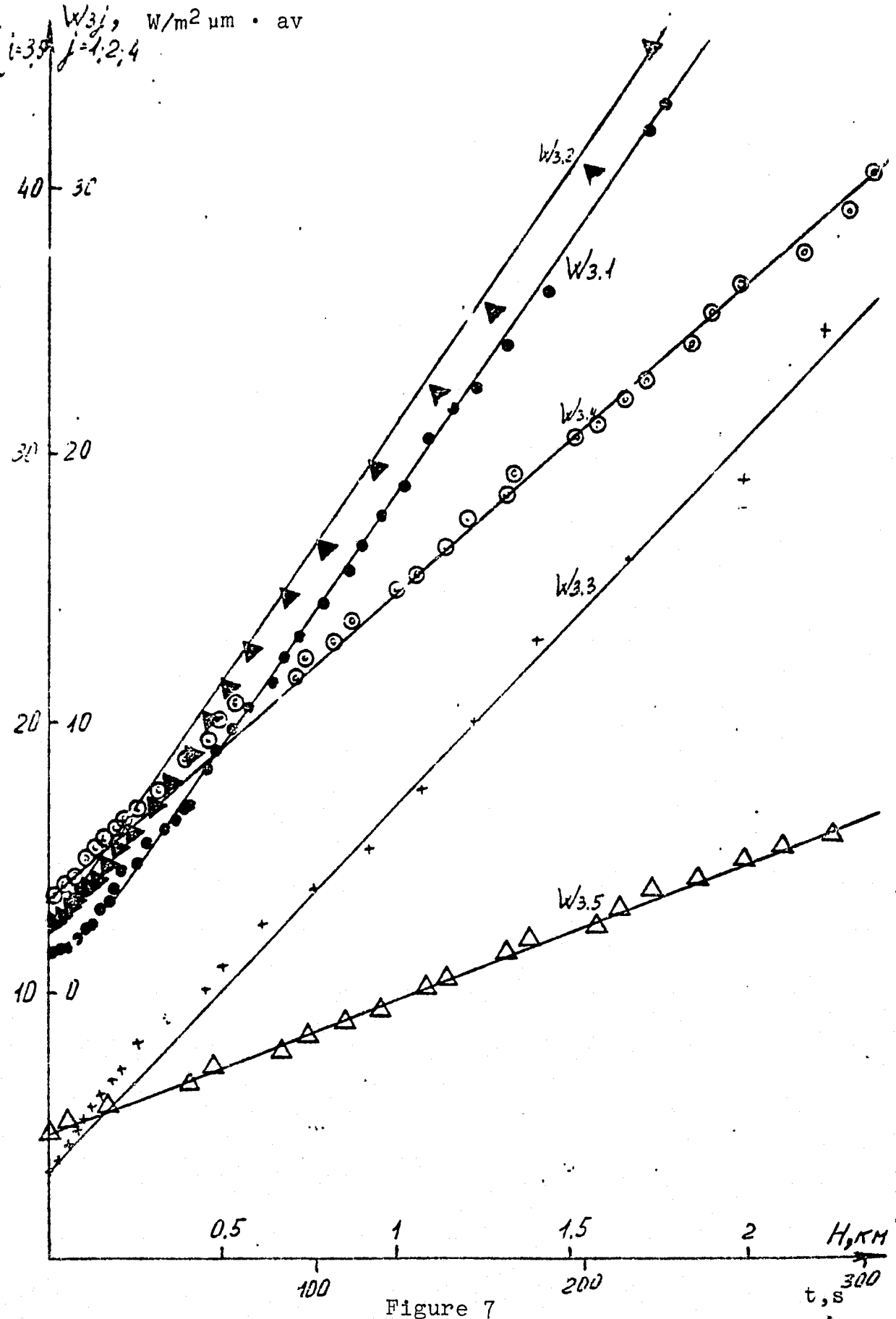
Figure 5

Figure 6

Figure 7
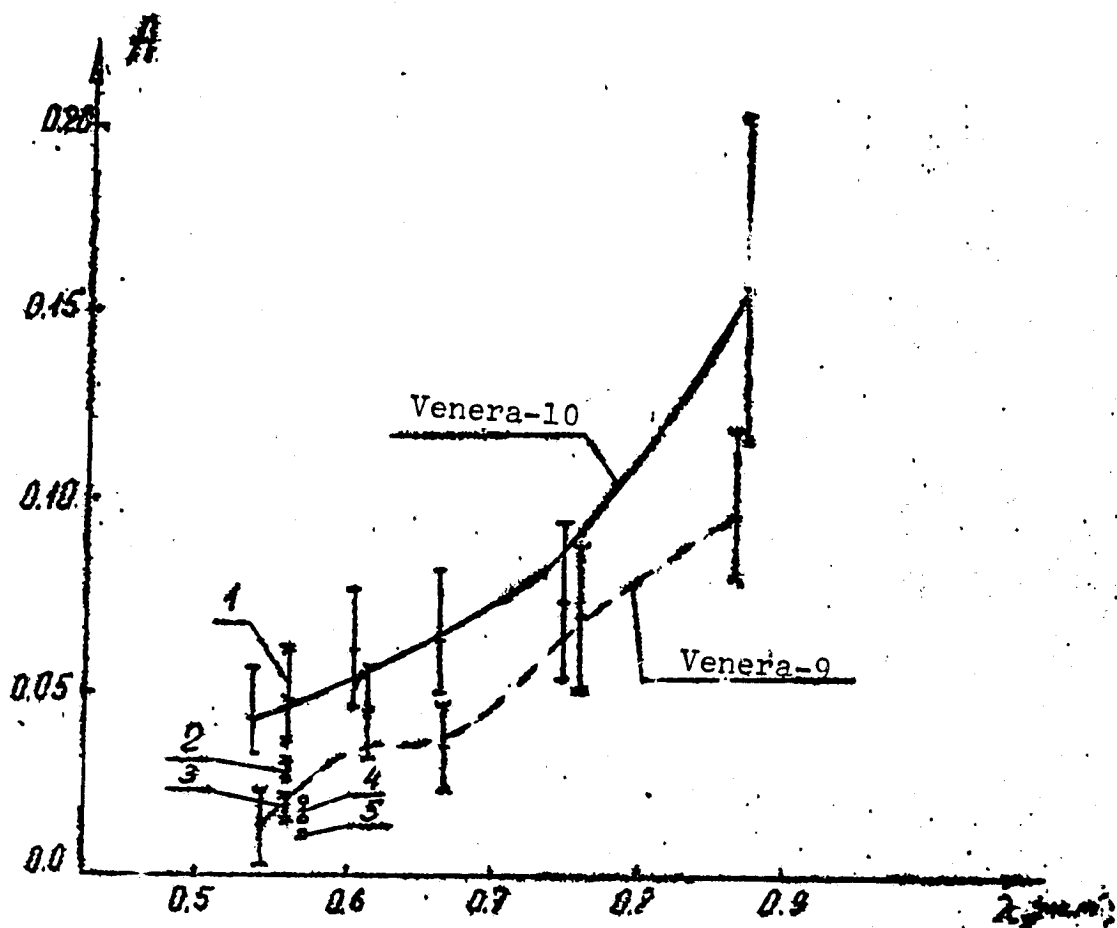
Figure 8
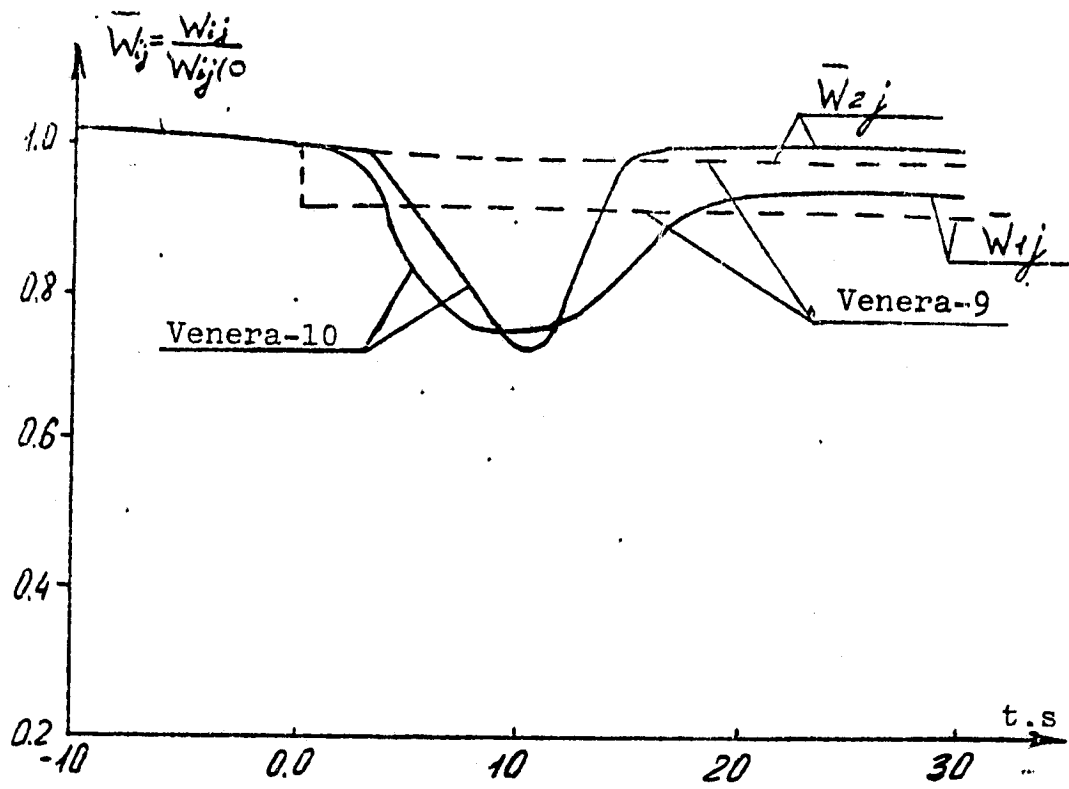
Figure 9
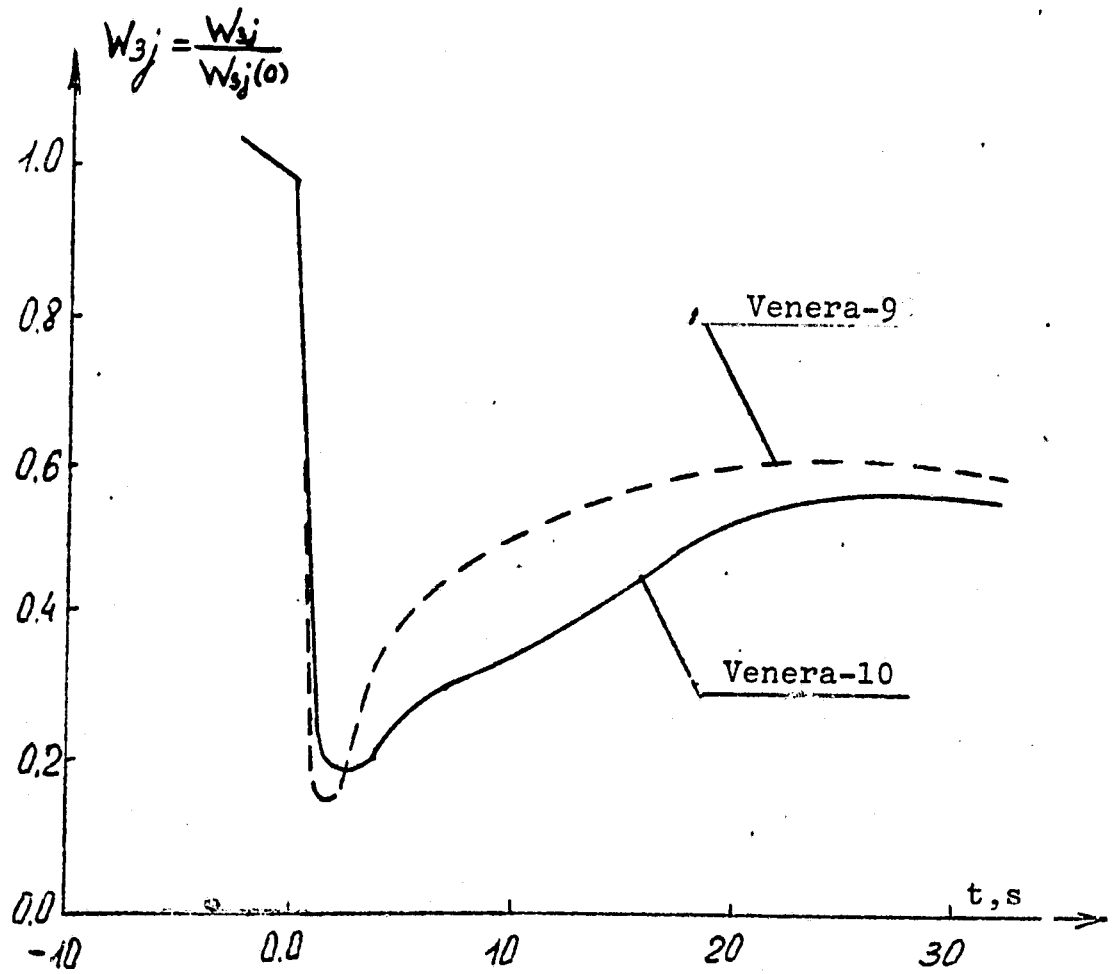
Figure 10
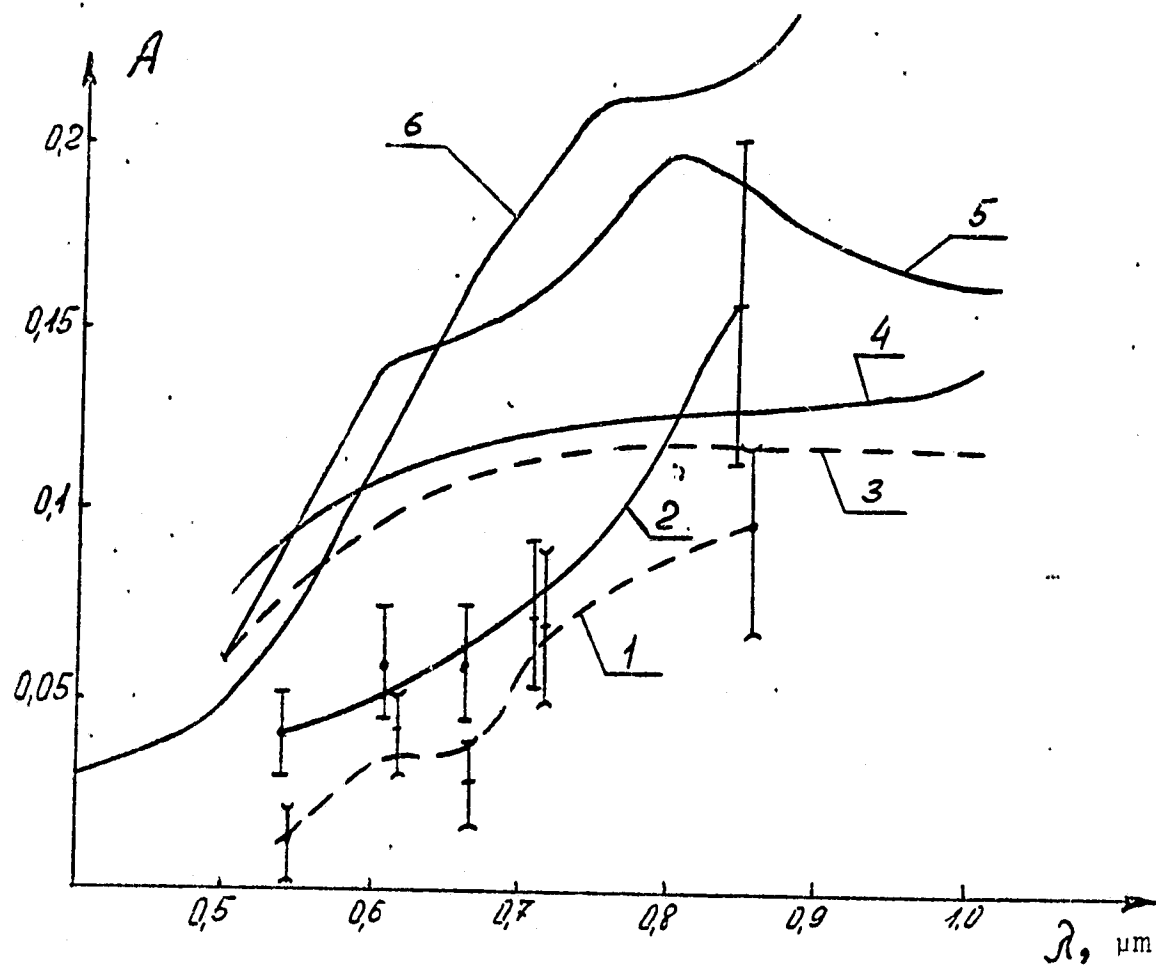
Figure 11

Figure 12

Figure 13

U_B

dust
cloud

a)

b)

c)
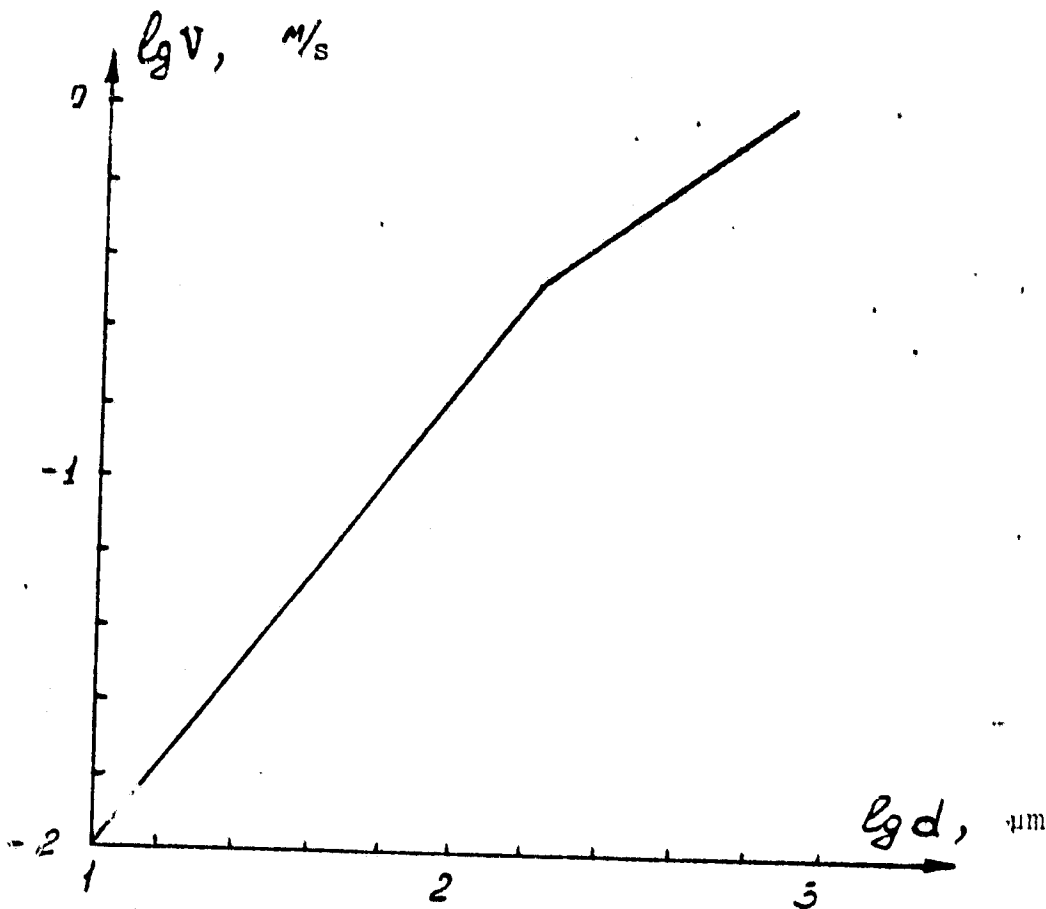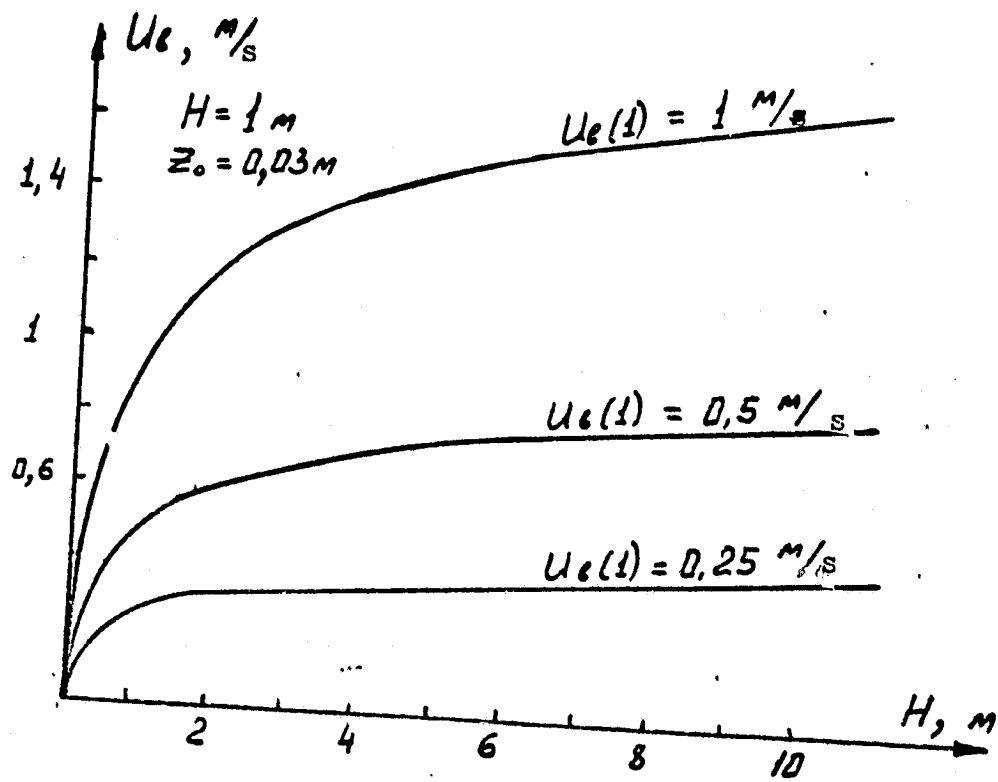
d)

e)

u

u
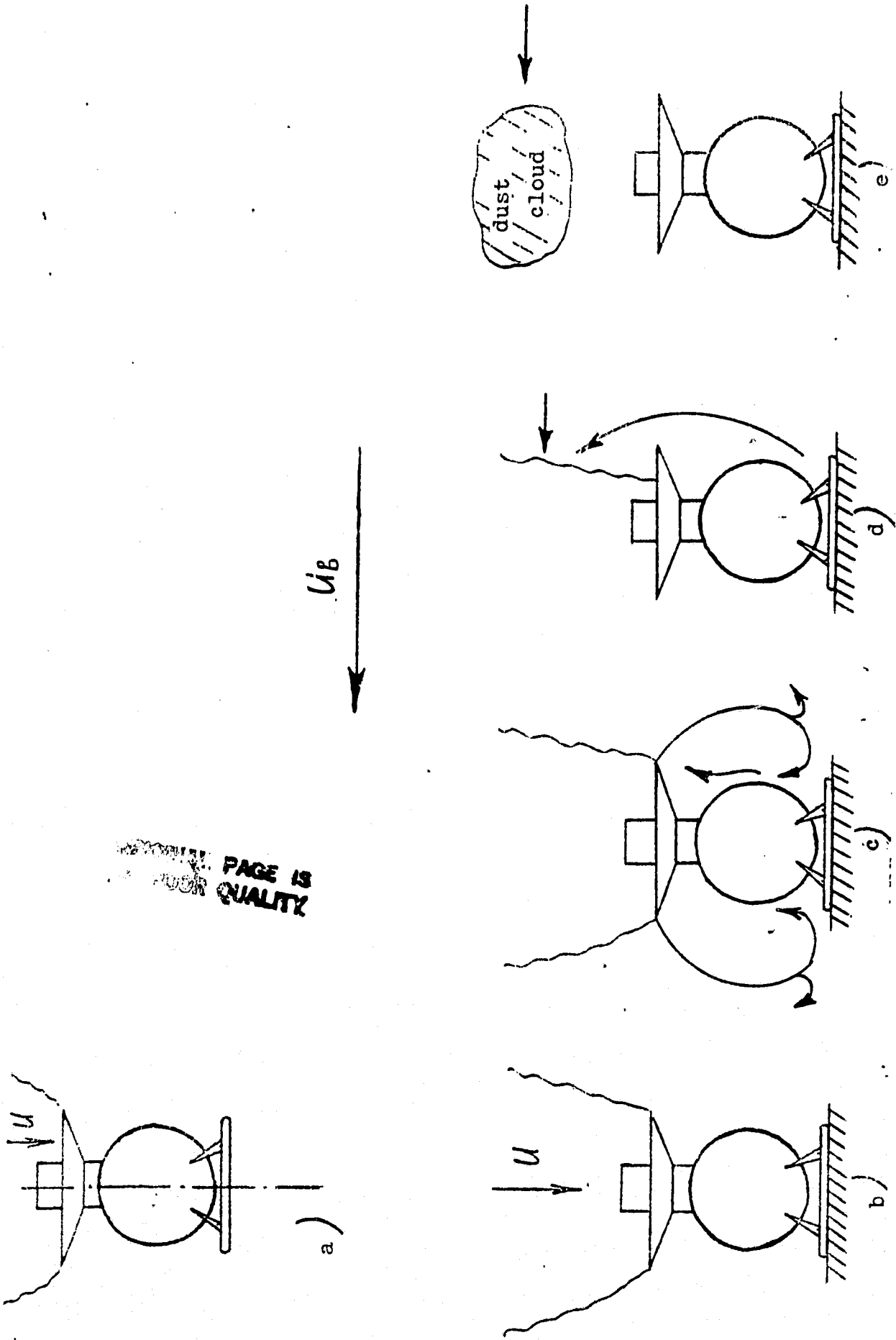
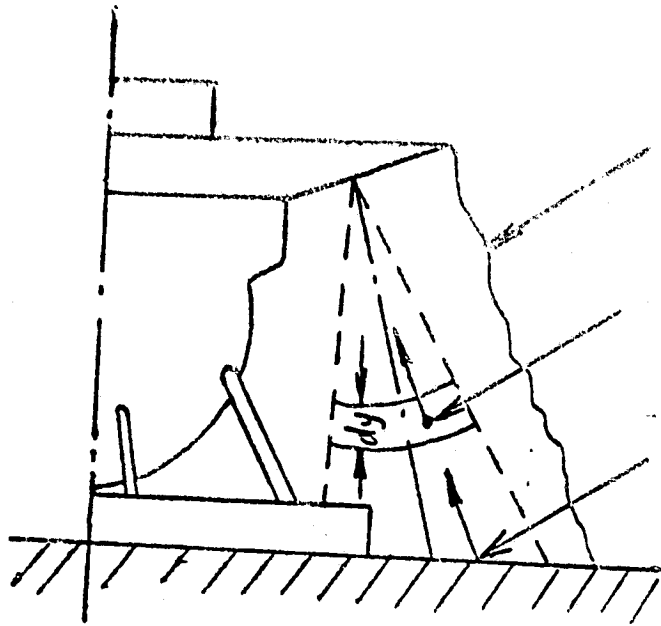Figure 14

Figure 15

Figure 16

Figure 17

Bibliography

1. Avduevskiy, V.S., Yu. M. Golovin, F.S. Zavelevich et al., _Dan SSSR_ 229/3, 579 (1976). /22

2. Avdievskiy, V.S., Yu. M. Golovin, F.S. Zavelevich et al., _Kosmich, issled._ 14/5, 735 (1976).

3. Sobolev, V.V., _Rasseyaniye sveta v atmosferakh planet_ [Scattering of light in the atmospheres of planets], Nauka Publ., 1972.

4. Panfilov, A.S. and A.I. Goron, _Kosmich. issled._ 14/5, 687 (1976).

5. _Tablitsy fizicheskiich velichin_ [Tables of physical value], Atomizdat Press, Moscow, 1976.

6. Marov, M. Ya. and O.L. Ryabov, "A model of the atmosphere of Venus," _IPM AN SSSR_, 39, (1972).

7. Avdueskiy, V.S., N.F. Borodin, V.P. Burtsev et al., _Kosmich. issled._ 14/5, 655 (1976).

8. _Atmosfery Zemli i planet_ [Atmospheres of the Earth and planets], Moscow, Inostrannaya Literatura Publ., 1951.

9. Fabelinskiy, I.L., _Molekulyarnoye rasseyaniye sveta_ [Molecular scattering of light], Moscow, Nauka Publ., 1965.

10. Selivanov, A.S., A.S. Panfilov et al., _Kosmich. issled._ 14/5, 678 (1976).

11. Selivanov, A.S., V.P. Chemodanov et al., _Kosmich. issled._ 14/5, 674 (1976.

12. Sharonov, V.V., _Astronom zh._ 42/1. 136 (1965).

13. Hovis, W.A., _Icarus_ 4, 425 (1965).

14. Adams, J.B. and A.L. Filise, _J. Geoph. Res._ 72, 5705 (1967).

15. Ross, H.P., J.E.M. Adler and G.R. Hunt, _Icarus_ 11, 46 (1969).

16. Adams, J.B. and T.B. McCord, _J. Geoph. Res._ 74, 4851 (1969).

17. Hunt, G.R. and H.P. Ross, _Applied Optics_ 6, 1687 (1967).

18. Rutten, M., _Proiskhozhdeniye zhizni_ [The origin of life], Mosocw, Mir Publ., 1973. /23

19. Surkov, Yu. A., F.F. Kirnozov at al., _Kosmich. issled._ 14/5, 697 (1976).

20. Surkov, Yu. A., F.F. Kirnozov et al., _Kosmich. issled._ 14/5. 704 (1976).

21. Moroz, V.I., _Kosmich. issled._ 14/1, 85 (1976).

22. Shlikhting, G., _Teoriya pogranichnogo sloya_ [Theory of a boundary layer], Nauka Publ., Moscow, 1974.

23. Avduevskiy, V.S., S.L. Vishnevetskiy et al., _Kosmich. issled._ 14/5, 710 (1976).